

Spectrally Selective Nanocomposite Textile for Outdoor Personal Cooling

Lili Cai, Alex Y. Song, Wei Li, Po-Chun Hsu, Dingchang Lin, Peter B. Catrysse, Yayuan Liu, Yucan Peng, Jun Chen, Hongxia Wang, Jinwei Xu, Ankun Yang, Shanhui Fan, and Yi Cui*

Outdoor heat stress poses a serious public health threat and curtails industrial labor supply and productivity, thus adversely impacting the wellness and economy of the entire society. With climate change, there will be more intense and frequent heat waves that further present a grand challenge for sustainability. However, an efficient and economical method that can provide localized outdoor cooling of the human body without intensive energy input is lacking. Here, a novel spectrally selective nanocomposite textile for radiative outdoor cooling using zinc oxide nanoparticle-embedded polyethylene is demonstrated. By reflecting more than 90% solar irradiance and selectively transmitting out human body thermal radiation, this textile can enable simulated skin to avoid overheating by 5–13 °C compared to normal textile like cotton under peak daylight condition. Owing to its superior passive cooling capability and compatibility with large-scale production, this radiative outdoor cooling textile is promising to widely benefit the sustainability of society in many aspects spanning from health to economy.

Outdoor space is an inevitable part in our everyday life that accommodates various indispensable physical activities and industrial operations. However, one risk often encountered when performing outdoor activities is the exposure to excessive heat stress.^[1] It is reported that heat stress is the leading cause of mortality from natural hazards in the United States.^[2] Heat-resulted physiological and psychological effects also lead to reduction in industrial labor productivity and supply, which eventually impact the overall economy and social welfare,

especially in developing countries.^[3] In the context of global warming, the health and economic threats of outdoor heat stress will become more intense and frequent.^[4] Recent analysis estimated that the annual cost of heat-caused issues will reach \$2.4 trillion by 2030.^[5]

Outdoor cooling is therefore crucially needed in many aspects for a sustainable society, but remains a big challenge due to its open nature. Unlike indoor space where air conditioning can be easily implemented, it is impractical and uneconomical to cool the enormous open space in the outdoor environment using energy-intensive heating, ventilation, and air conditioning systems. A desired solution under these circumstances is localized cooling of the human body through the garments.

Recently, radiative cooling textile has been recognized as an attractive strategy because it exerts the innate ability of the human body to emit thermal radiation without the need of any energy input.^[6–8] For indoor environment, it has been demonstrated that infrared transparent textile can fully transmit the body radiation heat to allow passive personal cooling.^[6,7] Outdoor radiative cooling under direct sunlight, however, presents a remarkably greater challenge due to the addition of substantial external heating from solar irradiance ($\approx 1000 \text{ W m}^{-2}$) and appreciable internal body heat generation ($\approx 100 \text{ W m}^{-2}$). This requires a textile material that has selective response in solar and mid-infrared wavelengths. Such a stringent material property has not been achieved yet.

Here, we demonstrate the first spectrally selective nanocomposite textile for outdoor radiative cooling, which shows more than 90% reflection of solar irradiance and high transmission of the human body thermal radiation. We combine intrinsic material property and structural photonic engineering, and develop this novel textile material with selective spectral response by embedding zinc oxide nanoparticles (NPs) into nanoporous polyethylene (ZnO-PE). We experimentally show that ZnO-PE can enable simulated skin to avoid overheating by more than 10 °C, corresponding to a cooling power of more than 200 W m^{-2} , compared to conventional textile like cotton under typical outdoor environment with peak solar irradiance over 900 W m^{-2} . Furthermore, when sweat evaporation comes into play, our radiative cooling textile can still avoid overheating of the skin-simulating heater by up to 8 °C compared to cotton.

Dr. L. Cai, Dr. P.-C. Hsu, Dr. D. Lin, Y. Liu, Y. Peng, Dr. J. Chen,
Dr. H. Wang, J. Xu, Dr. A. Yang, Prof. Y. Cui
Department of Materials Science and Engineering
Stanford University
Stanford, CA 94305, USA
E-mail: yicui@stanford.edu

Dr. A. Y. Song, Dr. W. Li, Dr. P. B. Catrysse, Prof. S. Fan
E. L. Ginzton Laboratory
Department of Electrical Engineering

Stanford University
Stanford, CA 94305, USA

Prof. Y. Cui
SLAC National Accelerator Laboratory
Stanford Institute for Materials and Energy Sciences
2575 Sand Hill Road, Menlo Park, CA 94025, USA

 The ORCID identification number(s) for the author(s) of this article can be found under <https://doi.org/10.1002/adma.201802152>.

DOI: 10.1002/adma.201802152

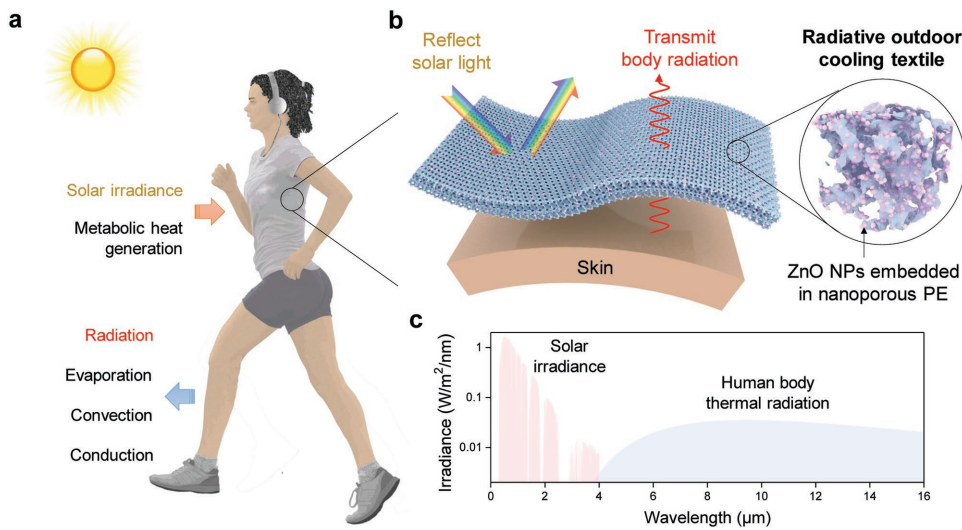


Figure 1. a) Schematic illustrating the heat input and output pathways of the human body under sunlight in outdoor environment. b) Schematic of the ZnO nanoparticle-embedded nanoporous PE textile, designed for radiative outdoor cooling by reflecting sunlight and transmitting human body thermal radiation. c) Spectra comparison of AM 1.5G solar irradiation^[10] and human body thermal radiation simulated using Planck's law at the skin temperature of 34 °C,^[11] showing that they have marginal overlapping of the wavelength range.

These results demonstrate the superior capability of combining thermoregulation concept with nanophotonic structure for passive outdoor personal cooling. We believe this will lead to revolutionary improvement of personal thermal management that can benefit not only individual health but also industrial productivity in a sustainable manner.

The heat exchange between human body and outdoor environment is illustrated in Figure 1a. The total heat stress on the human body can be defined as

$$P_{\text{heat stress}} = P_{\text{gen}} + P_{\text{sun}} - P_{\text{rad}} - P_{\text{evap}} - P_{\text{conv}} - P_{\text{cond}} \quad (1)$$

where P_{gen} is the metabolic heat generation rate, P_{sun} is the heat gain rate from solar irradiance, P_{rad} , P_{evap} , P_{conv} and P_{cond} are the net heat loss rates through radiation, evaporation, convection, and conduction, respectively.

Maintaining outdoor thermal comfort therefore involves the minimization of heat stress by reducing heat gain and enhancing heat loss. Conventional approaches mainly focus on the evaporative and convective heat loss of the garments to achieve outdoor cooling,^[9] but these two heat dissipation pathways have their own limitations that strongly depend on the environment conditions, such as humidity and wind levels. The solar irradiance and thermal radiation terms have been less considered for the textile, despite their large contributions to the overall heat exchange. As shown in Figure 1c, the solar irradiance spectrum (AM 1.5G) is mainly distributed in the visible and near-infrared range spanning from 0.3 to 4 μm with a total power density of about 1000 W m⁻².^[10] More than 60% of the total solar irradiance can be absorbed by the bare skin based on its averaged solar reflectivity value (Figure S1, Supporting Information). On the other side, human skin is a good IR emitter with an IR emissivity of 0.98 (Figure S1, Supporting Information). At the skin temperature of 34 °C, human body emits thermal radiation mainly in the mid-infrared range between 7 and 14 μm with the peak emission at the wavelength of 9.5 μm

and a net radiation power density of about 100 W m⁻².^[11] This infrared radiation range overlaps with the infrared transparency window of the earth's atmosphere. Thus, the thermal radiation from the human body can directly pass through the atmospheric window to the cold outer space (3 K) for heat dissipation. However, normal textile like cotton has low IR transmissivity that impedes efficient dissipation of human body thermal radiation (Figure S2, Supporting Information). In the meantime, the averaged solar reflectivity for cotton (white) is only about 60%, allowing large portion of the solar irradiance power to be absorbed by the skin (Figure S2, Supporting Information). Because of marginal overlapping between the solar irradiance and human body thermal radiation spectra, we propose a spectrally selective radiation textile material with strong solar reflection and high mid-infrared transmission to simultaneously minimize input and maximize output of radiative heat transfer for outdoor cooling.

Figure 1b shows the schematic of the proposed outdoor radiative cooling textile, which is composed of ZnO-PE matrix. PE, composed of only aliphatic C-C and C-H bond, was previously found to be IR-transparent, and thus can fully transmit out human body radiation for indoor cooling.^[6] Its solar reflectance is not satisfactory for outdoor purpose though, due to its relatively low refractive index $n \approx 1.5$.^[12] Inorganic solids typically have higher refractive index than polymers, but often have some visible or mid-infrared absorption. ZnO is a distinctive one that not only has high refractive index $n \approx 2$,^[13] but also has little absorption from visible (400 nm) up to mid-infrared wavelengths (16 μm).^[14] These intrinsic material properties render the combination of ZnO and PE uniquely suitable as the base material for constructing the desired radiation selectivity for outdoor cooling purpose.

We further numerically optimized the inorganic-organic matrix design using structural photonic engineering to derive the spectrally selective radiation property (detailed in the Supporting Information). Figure 2a simulates the normalized

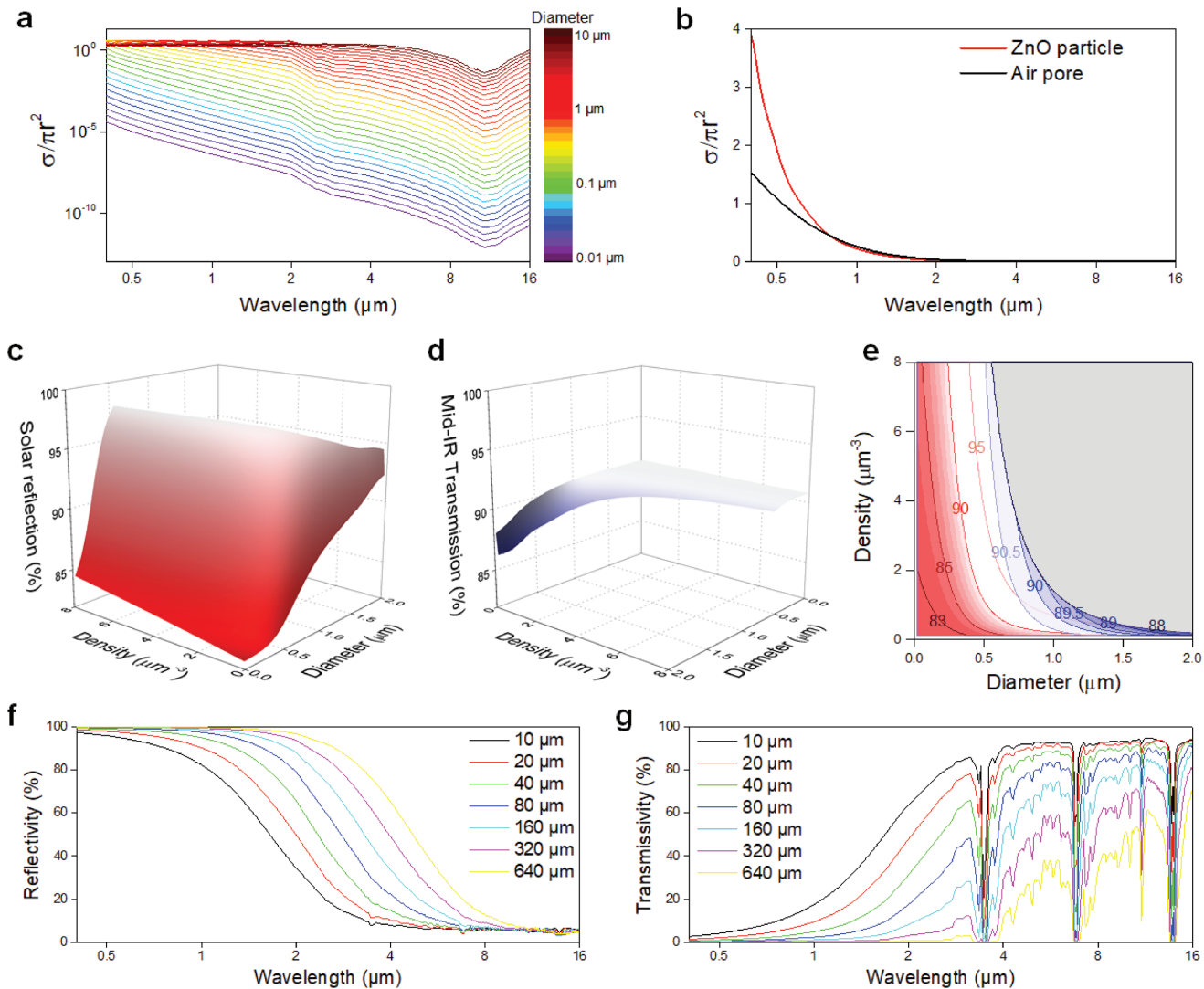


Figure 2. a) Simulation of the normalized scattering cross sections of a single ZnO particle in the medium of PE over the wavelength range of 0.4–16 μm with the particle diameter varied from 0.01 to 10 μm . b) Comparison of the normalized scattering cross sections between a ZnO particle and an air pore with the same diameter of 320 nm in the medium of PE. Dependence of the c) solar reflection and d) mid-infrared transmission of multiple ZnO particle-embedded nanoporous PE on the ZnO particle size and density. For each data point in (c) and (d), the scattering cross section is averaged for a normal distribution of the particle size with a variance of $\pm 0.1 \mu\text{m}$. The solar reflection is averaged over the solar irradiance spectrum from 0.4 to 4 μm . The mid-infrared transmission is averaged over the human body thermal radiation wavelength range from 4 to 16 μm . e) Projection of the 3D plots in (c) and (d) on the density versus size plane. The white regime presents the optimal densities and sizes of ZnO particles where both high solar reflection and high mid-infrared transmission can be achieved. Effect of the nanocomposite layer thickness on the f) solar reflection and g) mid-infrared transmission.

scattering cross sections of a spherical ZnO particle in the medium of PE over the spectral wavelengths from 0.4 to 16 μm with varying particle diameters from 0.01 to 10 μm . At particle sizes below 0.1 μm or above 1 μm , the scattering cross sections are either all small or all large over the whole wavelength ranges, resulting in minimal selectivity over the spectrum. At particle sizes between 0.1 and 1 μm , which are comparable to the wavelengths of solar light, strong Mie scattering occurs that significantly increases the scattering cross sections only in the visible and near-IR ranges, while the scattering in mid-IR remains small. This result suggests that proper selection of ZnO particle size within 0.1–1 μm is very critical toward

achieving high reflection in visible and near-IR region and high transmission in mid-IR region. In addition, we compared the scattering cross sections of a ZnO particle and an air pore in PE medium at the same diameter (i.e., 320 nm, Figure 2b). The comparison shows that the ZnO particle induces stronger scattering in the visible range than the air pore, further illustrating the advantage of ZnO for attaining higher visible reflectance. Finally, we performed detailed calculation to determine the effects of ZnO particle size and density (Figure 2c,d) as well as nanocomposite layer thickness (Figure 2e,f) on the solar reflection and mid-IR transmission. With the increase of particle size and density, the solar reflection increases while the mid-IR

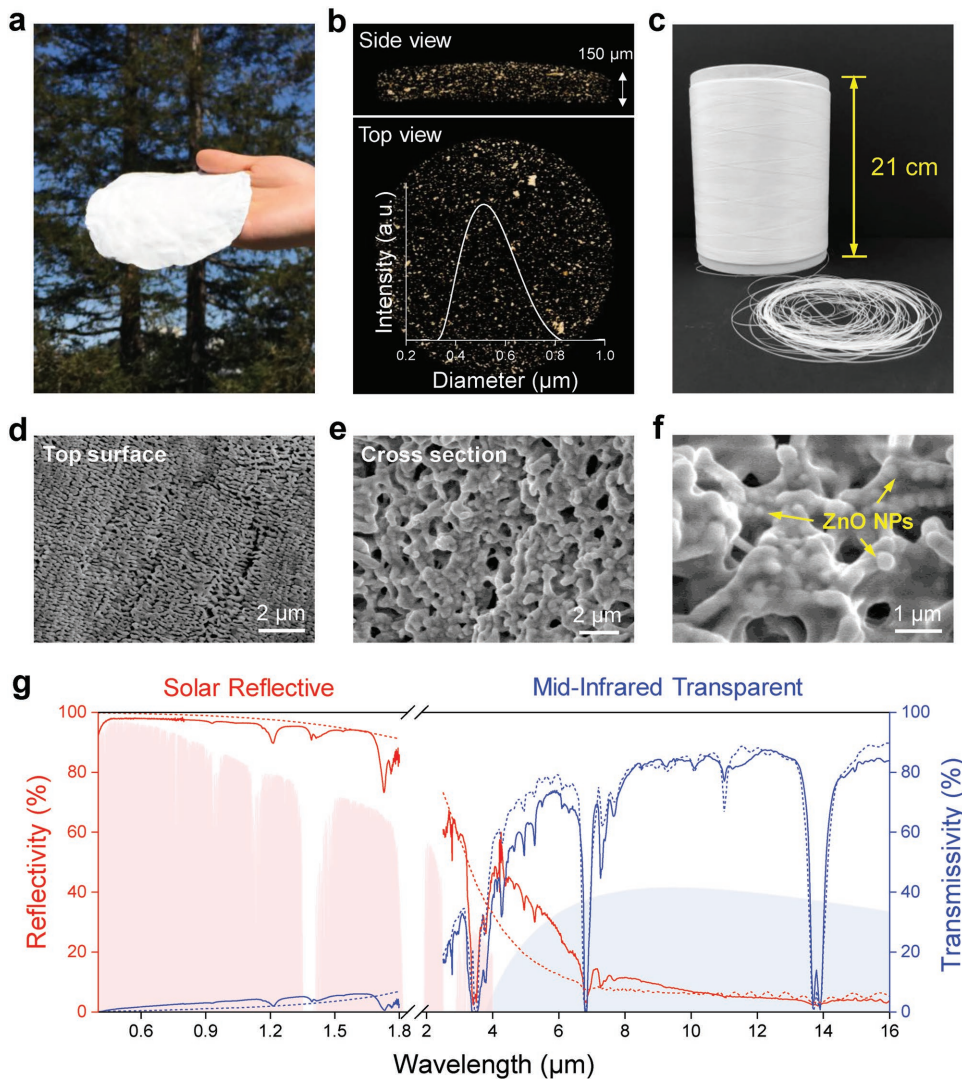


Figure 3. a) Photo of the ZnO-PE textile material under sunlight. b) Side view and top view of the X-ray computed tomographic image for the ZnO-PE sample, showing the uniform distribution of ZnO particles. Inset is the distribution profile of ZnO particle diameters measured using dynamic light scattering, which peaks at about 500 nm. c) Photo of a roll of ZnO-PE fibers made by melt-extrusion. SEM images showing the d) top surface and e) cross section of the ZnO-PE film sample. f) High-magnification SEM image showing the morphology of individual ZnO particles. g) Reflectivity and transmissivity spectra of ZnO-PE from ultraviolet to mid-infrared range (0.3–16 μm) from measurement with integrating spheres (solid lines) and simulation (dashed lines). The shaded areas show the AM 1.5G solar spectrum (pink) and human body radiation spectrum (blue) for reference.

transmission decreases, leading to an optimized range (white region) projected in Figure 2e. Similar tradeoff is also observed with the increase of nanocomposite layer thickness, where a thickness in-between 80 and 160 μm will be optimal for simultaneously high solar reflection and mid-IR transmission.

Given the guidance from numerical optimization, we experimentally fabricated the ZnO-PE textile material by mixing ZnO particles with melted PE at a weight ratio of ZnO:PE = 2:5 in paraffin oil (ratio of PE to oil is 1:5), then melt-pressing the composite mixture into a thin film, and finally extracting out the paraffin oil from the film with methylene chloride. Note that methylene chloride is very volatile and can be completely removed by evaporation. No residual methylene chloride was detected from the textile sample after 2 h drying in air (Figure S3, Supporting Information). The resulting ZnO-PE

film with a thickness of 150 μm shows white color under the sun (Figure 3a), implying strong scattering of all visible light from all angles. Examination under scanning electron microscopy (SEM) revealed the porous structure of the textile material (the pore occupation volume is 20–30%) with ZnO NPs randomly embedded in the PE matrix (Figure 3d–f). X-ray computed tomographic scanning of the textile sample using X-ray microscope showed a uniform distribution of ZnO particles within the whole volume (Figure 3b). Their diameters were characterized using dynamic light scattering to be mainly between 0.3 and 0.8 μm with a peak at about 0.5 μm (Figure 3b), matching with the numerically optimized particle size. Besides, inductively coupled plasma-mass spectrometry (ICP-MS) measurement was conducted to quantify Zn²⁺ concentration in the water before and after washing the ZnO-PE

textile material with detergent and stirring force for 30 min. Figure S4 (Supporting Information) shows that trace amount of ZnO (≈ 2 ppb) was released into the water during the washing cycle. This demonstrates the good durability of the embedding structure, due to intimate wrapping of PE over ZnO particles.

The optical properties of ZnO-PE were measured using ultra-violet–visible–near infrared (UV–vis–NIR) and Fourier transform infrared (FTIR) spectroscopies with integrating spheres. The measured spectra show high reflectivity of more than 90% in the solar light region and high transmissivity of $\approx 80\%$ between 7 and 14 μm where the human body thermal radiation is centralized (Figure 3g). The measured spectra overall match very well with the theoretical simulation results, validating our strategic selection of proper materials and structural photonic design for the realization of such unique spectrally selective feature to satisfy the requirement of radiative outdoor cooling textile. Note that in the simulation, we have only considered the scattering response from the electric and magnetic resonances in the particles with different diameters. There are still some differences between experiment and simulation, for example, in the wavelength region of 4–6 μm . This discrepancy may result from the collective excitation of coupled electric and magnetic dipoles.^[15,16]

Our design here builds upon existing daytime radiative cooling strategy and further expands the possibilities from buildings/solar absorbers to human body.^[17] Zhai et al.,^[16] Raman et al.,^[18a] and Goldstein et al.^[18b] achieved outdoor radiative cooling of the building roof below the ambient air temperature, with a use of layer that has strong thermal emission and strong solar reflection. Zhu et al.^[19a] and Li et al.^[19b] aimed to achieve radiative cooling of a solar absorber such as a solar cell, with the use of layer that has strong thermal emission and high solar transmission in order to preserve the solar absorption properties of the cell. In contrast, here with the aim of achieving outdoor human body cooling, the textile layer we use here, by itself, has very low thermal emission (high thermal transmission instead) and strong solar reflection. Its radiation property is quite different from existing approaches for radiative cooling, and our work here further highlights the diverse opportunities of radiative cooling depending on the nature of the applications. More importantly, our approach is specifically designed for textile applications with a distinctive feature that the material can be extruded into fibers for knitting or weaving of textiles (Figure 3c).

We then demonstrated the outdoor performance of the ZnO-PE radiative cooling textile on clear spring days in Stanford, California. The measurement setup shown in Figure 4a consists of a heater simulating the skin, which is placed on top of a foam to prevent heat loss to the bottom, a thermocouple on the heater surface to measure the simulated skin temperature, and a textile sample covering the simulated skin (Figure 4b). A heating power input of 104 W m^{-2} was applied to the heater to simulate the metabolic heat generation rate of the skin. The real-time temperature of skin-simulating heater was recorded for 4 h around noon time, while the whole setup was under direct sunlight and exposed to the air. As shown in Figure 4c, under wind convection (wind speed: 8 km h^{-1} , relative humidity: 50%) and peak solar irradiance of 910 W m^{-2} around 13:00 (local time), ZnO-PE-covered skin-simulating

heater displayed a temperature of 33.5 °C, much lower than those of white cotton-covered (45.6 °C) and bare (53.1 °C) skin-simulating heaters. Note that the temperatures of these skin-simulating heaters without the textile samples were the same under both sunlight and shade (Figure S5, Supporting Information), confirming that the measured temperature differences came from the effect of the textiles. The notably lower temperature for ZnO-PE-covered skin-simulating heater exhibits the superior cooling power of ZnO-PE, ascribed to its high solar reflection that minimizes heat input from sun, as well as its high transmission to human body thermal radiation that maximizes radiative heat output. We calculated the additional cooling power demands by these textile samples to achieve normal skin temperature of 34 °C under the test condition in Figure 4c using heat transfer model analysis (detailed in Figures S6 and S7, Supporting Information). Over the day from 11:00 to 15:00 (local time), cotton-covered and bare skin-simulating heaters required additional cooling powers of 116–219 W m^{-2} and 305–454 W m^{-2} , respectively, while ZnO-PE instead passively cooled the skin-simulating heaters to maintain the temperature slightly below 34 °C without the need of additional cooling power supply (Figure 4d).

We further considered that sweat evaporation could provide the additional cooling power, which was estimated as the product of the water evaporation rate through the textile (Figure S8, Supporting Information) and the heat of vaporization of water (44 kJ mol^{-1}).^[20] Note that the water evaporation rate through ZnO-PE ($0.02 \text{ g m}^{-2} \text{ s}^{-1}$) is much lower than those through cotton ($0.03 \text{ g m}^{-2} \text{ s}^{-1}$) and from bare skin ($0.12 \text{ g m}^{-2} \text{ s}^{-1}$). This is mainly due to the non-woven structure and surface hydrophobicity of ZnO-PE. However, the estimated cooling power supply by evaporation still cannot compensate the cooling power demands by cotton-covered and bare skin-simulating heaters under wind convection and peak solar irradiance of 910 W m^{-2} (Figure 4f). We also performed real-time outdoor measurement under wind convection (wind speed: 16 km h^{-1} , relative humidity: 68%) and solar irradiance of 900–1050 W m^{-2} with a water-soaked porous layer on top of the heater to take the sweat evaporation effect into account (Figure 4e). With the addition of sweat evaporation effect, ZnO-PE still maintains the temperature of skin-simulating heater around 34 °C, while overheating by 5–8 °C and 9–15 °C resulted for cotton-covered and bare cases, respectively, which is consistent with the thermal analysis results, and further confirms the superiority of radiative cooling in outdoor environment.

In summary, our work developed a novel ZnO-PE nanocomposite textile with spectrally selective radiation properties favorable for passive outdoor cooling of the human body through the combination of intrinsic material properties and structural photonic engineering. The remarkable outdoor cooling performance demonstrated here displays the prominence of radiative heat dissipation mechanism, a missing feature in conventional textiles, for confronting the enormous challenge of increasingly intense and frequent outdoor heat stress with warming climates. Like other man-made textile materials (e.g., nylon and polyester), wearability modification treatments can be applied to ZnO-PE to improve the wearing comfort for practical use. Further engineering the fiber shape, surface hydrophilicity (e.g., by polydopamine coating) and

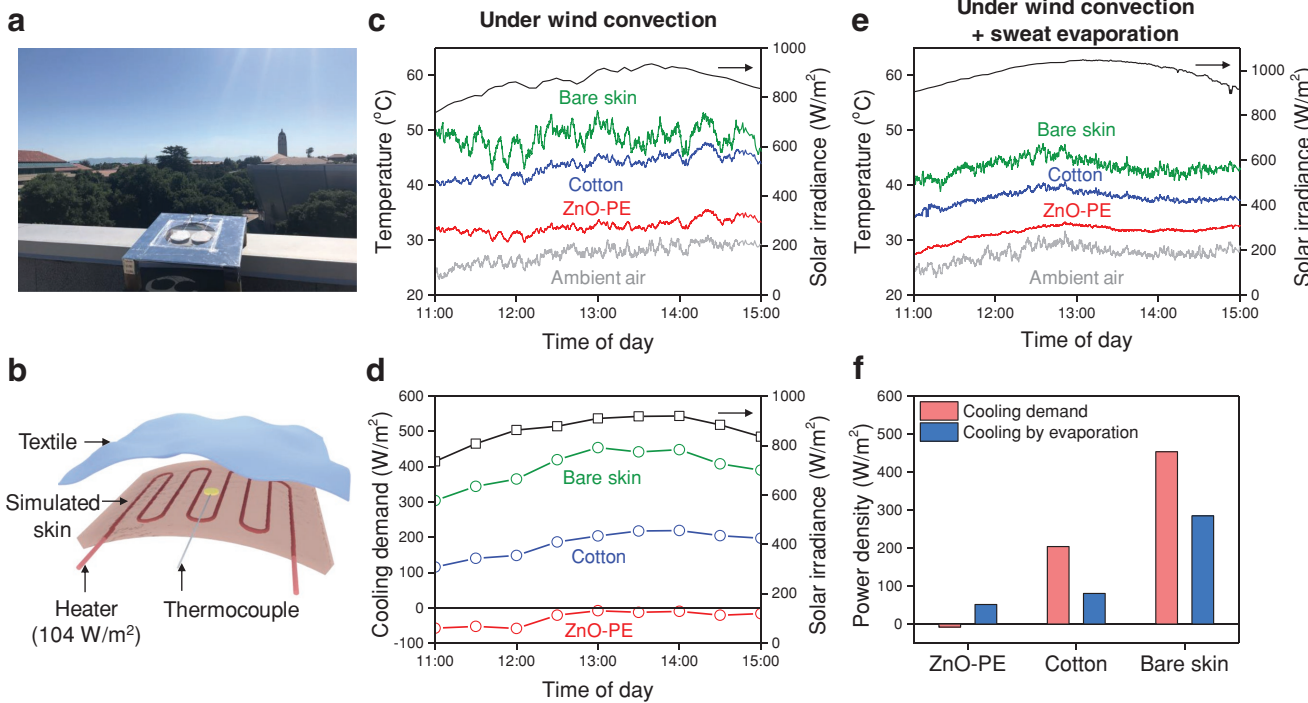


Figure 4. a) Photo of the thermal measurement setup in the outdoor test environment. b) Schematic of the thermal measurement setup consists of a heater simulating the skin, a thermocouple measuring the simulated skin temperature, and a textile sample covering the simulated skin. c) Comparison of the temperatures measured with ZnO-PE-covered, cotton-covered, and bare skin-simulating heaters under wind convection over a duration of 4 h on a clear spring day in Stanford, California. Ambient temperature and solar irradiance are measured and plotted for reference. d) Calculated additional cooling power demands by ZnO-PE-covered, cotton-covered, and bare skin-simulating heaters to maintain the normal skin temperature of 34 °C based on the measurement results in (c). e) Comparison of the temperatures measured with ZnO-PE covered, cotton-covered, and bare skin-simulating heaters under wind convection and sweat evaporation. f) Comparison of the cooling power demands at 13:00 (local time) in (d) and the cooling power supplies by sweat evaporation, estimated as the product of the water evaporation rate through the textile (Figure S8, Supporting Information) and the heat of vaporization of water, for ZnO-PE-covered, cotton-covered, and bare skin-simulating heaters.

weaving/knitting pattern of ZnO-PE to incorporate the moisture wicking property will further improve the cooling efficiency by cooperative function of both radiative and evaporative heat dissipation. Given its practical compatibility with large-scale fabrication, it is anticipated that this radiative outdoor cooling textile will push forward transformative change of personal thermal management towards better health, productivity, and sustainability.

Experimental Section

Fabrication of ZnO-PE Radiative Outdoor Cooling Textile: The ZnO-PE composite material was fabricated by mixing ZnO particles (99.9%, Sigma Aldrich) with high-density PE (HDPE, melt index 2.2 g/10 min, Sigma Aldrich) and ultrahigh molecular weight PE (UHMW, Alfa Aesar) at a weight ratio of ZnO:HDPE:UHMWPE = 2:4:1 in paraffin oil (light, Fisher Chemical) at the temperature of ≈200 °C. The volume of paraffin oil was five times the weight of PE. The mixture was then melt-pressed into a thin film at 70–100 °C. Finally, the paraffin oil was extracted out from the film using methylene chloride (99.99%, Fisher Chemical). The ZnO-PE fibers were melt-extruded using a commercial extruder.

Material Characterizations: The SEM images were taken by FEI Sirion (5 kV). The X-ray computed tomographic scanning was performed using ZEISS Xradia 520 Versa X-ray microscope. The ZnO particle diameter distribution profile was characterized using Malvern Zetasizer Nano ZS. The UV-vis-NIR reflectivity and transmissivity were measured

using Agilent Cary 6000i UV-vis-NIR spectrophotometer with a diffuse integrating sphere. The IR reflectivity and transmissivity were measured using an FTIR spectrometer (Model 6700, Thermo Scientific) accompanied with a diffuse gold integrating sphere (PIKE Technologies).

Outdoor Thermal Measurements: The skin was simulated using a silicone rubber insulated flexible heater (Omega, 39 cm²). The heater was connected to a power supply (Keithley 2400) which provided a heating power density of 104 W m⁻² to simulate the metabolic heat generation rate. An insulating foam was placed below the simulated skin heater to ensure that the heat generated by the skin heater only transfers to the ambient environment. A ribbon-type hot junction thermocouple (0.3 mm in diameter, K-type, Omega) was in contact with the top surface of the heater to measure the simulated skin temperature. The textile sample covered over the skin-simulating heater. The whole device was supported by a wooden frame covered with a layer of aluminized Mylar. During the test, the setup was exposed to direct sunlight and air. The real-time temperatures for ZnO-PE-covered, cotton-covered, and bare skin-simulating heaters, as well as the ambient temperature, were measured. Direct and diffuse solar irradiance was recorded using a pyranometer (Kipp&Zonen CMP 6). For measurements with the sweat evaporation effect, a thin layer of carbon-coated aluminum foam was soaked with water, sealed with a polydopamine-coated nanoPE film, and placed on top of the heater to simulate the sweat evaporation effect.

Water Evaporation Rate Test: This test procedure was based on ASTM E96 with modification. 100 mL media bottles (Fisher Scientific) were filled with 40 mL distilled water and then sealed by the textile samples using open-top caps and silicone gaskets (Corning). The sealed bottles were then placed into an environmental chamber. The temperature and

relative humidity inside the chamber were held at 35 °C and 30 ± 10%, respectively. The total mass of the bottles together with the samples was measured periodically. The reduced mass, corresponding to the evaporated water, was then divided by the exposed area (3 cm in diameter) and the time to derive the water evaporation rate.

Supporting Information

Supporting Information is available from the Wiley Online Library or from the author.

Acknowledgements

L.C. and A.Y.S. contributed equally to this work. This work was sponsored by the Advanced Research Projects Agency-Energy (ARPA-E), US Department of Energy, under Award Number DE-AR0000533.

Conflict of Interest

The authors declare no conflict of interest.

Keywords

nanocomposite textile, radiation, spectrally selective, thermal management, zinc oxide

Received: April 3, 2018

Revised: June 10, 2018

Published online: July 17, 2018

- [1] a) R. S. Kovats, S. Hajat, *Annu. Rev. Public Health* **2008**, *29*, 41; b) J. T. Spector, D. K. Bonauto, L. Sheppard, T. Busch-Isaksen, M. Calkins, D. Adams, M. Lieblich, R. A. Fenske, *PLOS One* **2016**, *11*, e0164498.
- [2] G. Luber, M. McGeehin, *Am. J. Prev. Med.* **2008**, *35*, 429.
- [3] a) A. P. C. Chan, W. Yi, *Indoor Built Environ.* **2016**, *25*, 3; b) T. Kjellstrom, D. Briggs, C. Freyberg, B. Lemke, M. Otto, O. Hyatt, *Annu. Rev. Public Health* **2016**, *37*, 97.

- [4] a) B. Jones, B. C. O'Neill, L. McDaniel, S. McGinnis, L. O. Mearns, C. Tebaldi, *Nat. Clim. Change* **2015**, *5*, 652; b) P. B. Duffy, C. Tebaldi, *Clim. Change* **2012**, *111*, 487.
- [5] DARA and the Climate Vulnerable Forum, *Climate Vulnerability Monitor: A Guide to the Cold Calculus of a Hot Planet*, 2nd ed., (Ed: M. McKinnon), DARA, Madrid, Spain **2012**, p. 331.
- [6] P.-C. Hsu, A. Y. Song, P. B. Catrysse, C. Liu, Y. Peng, J. Xie, S. Fan, Y. Cui, *Science* **2016**, *353*, 1019.
- [7] a) J. K. Tong, X. Huang, S. V. Boriskina, J. Loomis, Y. Xu, G. Chen, *ACS Photonics* **2015**, *2*, 769; b) A. Yang, L. Cai, R. Zhang, J. Wang, P.-C. Hsu, H. Wang, G. Zhou, J. Xu, Y. Cui, *Nano Lett.* **2017**, *17*, 3506.
- [8] a) P.-C. Hsu, X. Liu, C. Liu, X. Xie, H. R. Lee, A. J. Welch, T. Zhao, Y. Cui, *Nano Lett.* **2015**, *15*, 365; b) L. Cai, A. Y. Song, P. Wu, P.-C. Hsu, Y. Peng, J. Chen, C. Liu, P. B. Catrysse, Y. Liu, A. Yang, C. Zhou, C. Zhou, S. Fan, Y. Cui, *Nat. Commun.* **2017**, *8*, 496.
- [9] a) S. Sarkar, V. Kothari, *Indian Journal of Fibre & Textile Research* **2014**, *39*, 450; b) M. Mokhtari Yazdi, M. Sheikhzadeh, *J. Text. Inst.* **2014**, *105*, 1231.
- [10] ASTM G173-03 (2012), Standard Tables for Reference Solar Spectral Irradiances: Direct Normal and Hemispherical on 37° Tilted Surface, ASTM International, West Conshohocken, PA **2012**.
- [11] J. Steketee, *Phys. Med. Biol.* **1973**, *18*, 686.
- [12] A. Hamza, T. Sokkar, M. Mabrouk, M. El-Morsy, *J. Appl. Polym. Sci.* **2000**, *77*, 3099.
- [13] W. L. Bond, *J. Appl. Phys.* **1965**, *36*, 1674.
- [14] a) A. Smith, in *The Coblenz Society Desk Book of Infrared Spectra*, 2nd ed., (Ed: C. D. Carver), The Coblenz Society, Kirkwood, MO **1982**, pp. 1–24; b) V. Srikant, D. R. Clarke, *J. Appl. Phys.* **1998**, *83*, 5447.
- [15] a) C. Wang, Z. Y. Jia, K. Zhang, Y. Zhou, R. H. Fan, X. Xiong, R. W. Peng, *J. Appl. Phys.* **2014**, *115*, 244312; b) Z. Y. Jia, J. N. Li, H. W. Wu, C. Wang, T. Y. Chen, R. W. Peng, M. Wang, *J. Appl. Phys.* **2016**, *119*, 074302.
- [16] Y. Zhai, Y. Ma, S. N. David, D. Zhao, R. Lou, G. Tan, R. Yang, X. Yin, *Science* **2017**, *355*, 1062.
- [17] W. Li, S. Fan, *Opt. Express* **2018**, *26*, 15995.
- [18] a) A. P. Raman, M. A. Anoma, L. Zhu, E. Rephaeli, S. Fan, *Nature* **2014**, *515*, 540; b) E. Goldstein, A. P. Raman, S. Fan, *Nat. Energy* **2017**, *2*, 17143.
- [19] a) L. Zhu, A. P. Raman, S. Fan, *Proc. Natl. Acad. Sci. USA* **2015**, *112*, 12282; b) W. Li, Y. Shi, K. Chen, L. Zhu, S. Fan, *ACS Photonics* **2017**, *4*, 774.
- [20] W. M. Haynes, *CRC Handbook of Chemistry and Physics*, 97th ed., CRC Press, Boca Raton, FL **2016**.